

# Altitude-dependent polarization in radio pulsars

J. Dyks

*Nicolaus Copernicus Astronomical Center, Toruń, Poland*

Accepted 1988 December 15. Received 1988 December 14; in original form 1988 October 11

## ABSTRACT

Because of the corotation, the polarization angle (PA) curve of a pulsar lags the intensity profile by  $4r/R_{lc}$  rad in pulse phase. I present a simple and short derivation of this delay-radius relation to show that it is not caused by the aberration (understood as the normal beaming effect) but purely by contribution of corotation to the electron acceleration in the observer’s frame. Available altitude-dependent formulae for the PA curve are expressed through observables and emission altitude to make them immediately ready to use in radio data modelling. The analytical approximations for the altitude-dependent PA curve are compared with exact numerical results to show how they perform at large emission altitudes. I also discuss several possible explanations for the opposite-than-normal shift of PA curve, exhibited by the pedestal emission of B1929+10 and B0950+08.

**Key words:** pulsars: general – pulsars: individual: B1929+10 – B0950+08 – Radiation mechanisms: non-thermal.

## 1 INTRODUCTION

In the simplest model of pulsar polarization (Komesaroff 1970; Radhakrishnan & Cooke 1969, hereafter RC69) the position angle of polarization does not depend on the radial distance<sup>1</sup> of radio emission  $r$ . The polarization angle (PA) becomes dependent on  $r$  when dynamic effects of pulsar’s rotation are taken into account (dragging of electrons by the corotating magnetic field). Blaskiewicz et al. (1991) (hereafter BCW) showed that if the emission originates from a fixed radial distance  $r$ , the shape of the PA swing is (approximately) preserved (ie. it is the same as in the case of negligible  $r$ ), but the entire swing is shifted towards later phases by  $\Delta\phi_{BCW} \approx 4r/R_{lc}$  radians with respect to the center of the profile (where  $R_{lc}$  is the light cylinder radius). Following BCW, I will refer to this formula with the term ‘delay-radius’ relation. Hibschiemann & Arons (2001) (hereafter HA) have shown that the PA curve also undergoes vertical shifts, ie. in the PA values. Both these results appear to have interesting observational consequences (eg. Ramachandran & Kramer 2003; von Hoensbroech & Xilouris 1997).

In the case of phase-dependent emission altitude different parts of the PA curve undergo different shifts and the PA curve assumes a distorted shape. This effect regularly happens to be employed to model observed distortions of PA curves and to derive magnetospheric emission altitudes (eg. Krishnamohan & Downs 1983, hereafter KD83; Xu, Qiao & Han 1997; Gil & Krawczyk 1997; Mitra & Seiradakis

2004). A tool that is needed for this is an analytical formula for the PA that explicitly depends on the radial distance of the emission region. BCW and HA provide various forms of this equation. However, their formulae are not in a ready-to-use form: they are expressed through the emission time instead of the pulse longitude  $\phi_{obs}$  (hereafter called pulse *phase*<sup>2</sup>). It is the need for this last step of the BCW’s analysis that actually sparked writing of this paper.

A strict and formal description of the PA subject is given in the superb work of Hibschiemann & Arons (2001; see their appendices) and it will not be repeated in this paper. My intention here is to provide a simple reference for those who want to use the altitude-dependent PA curves in their data modelling. The aim is to clarify some obscure aspects of the subject by trivialising the formalism and to provide practical PA equations in their final form. Accordingly, Sect. 2 presents a very simple and short derivation of the delay-radius relation to clearly expose its origin. In Sect. 3 I introduce the fiducial phase, describe the magnitudes and directions of various relativistic shifts with respect to it, and I write down the equations for the altitude-dependent PA curve in a form that is ready for immediate use in data modelling. In Sect. 4 I compare the analytical approximations to exact numerical results obtained for various emission altitudes to show the validity range of the BCW theory. In Sects. 4.4 and 4.5 I discuss possible explanations for the opposite-than-expected shifts of PA curve, as

<sup>1</sup> The quantity  $r$  represents the distance measured from the *center* of the neutron star.

<sup>2</sup> Throughout this paper the phase is assumed to be measured in radians whenever dimensionless terms are added to it.

exemplified by the pedestal radio emission components of B1929+10 and B0950+08. These and other interpretations of the anti-BCW shifts are summarized in Sect. 5.

## 2 SIMPLE DERIVATION OF THE DELAY-RADIUS RELATION DUE TO COROTATION

The derivation presented here is constrained to the case of the equatorial<sup>3</sup> plane of an orthogonally rotating pulsar (with dipole inclination  $\alpha = 90^\circ$ ). However, it is simple, intuitive and demonstrates the effect more directly than the original derivation of BCW.

Because of their corotation, trajectories of electrons are bent forward (toward the direction of rotation) in the inertial observer frame (IOF) with respect to trajectories in the corotating frame (CF). The trajectory of electrons that move along the dipole axis acquires some forward curvature, whereas the rectilinear motion occurs somewhere on the trailing side of the dipole axis. The bundle of IOF-trajectories becomes approximately symmetric around the location of this straight trajectory, which now assumes the role that the dipole axis had in the RC69 model (RVM model). This zero-curvature trajectory is associated with the inflection point of the PA curve. Its location can be found in the following two steps. First, we calculate ‘rotationally-induced curvature’, which is understood as the curvature imposed by rotation on a trajectory that is a straight line in the CF. Second, we will search for a place on the trailing side of the dipole axis, where this rotational curvature is exactly cancelled by the same-magnitude backward curvature of dipolar magnetic field lines.

Relativistic electrons (with the speed of essentially constant magnitude  $v \simeq c$ ) that move radially along the dipole axis in the frame rotating with the neutron star’s angular velocity  $\Omega$ , undergo acceleration  $a \simeq 2\Omega c$  in the IOF. This result can be obtained in several elementary ways (see the exercise in Appendix A). The particle trajectory along the dipole axis thus acquires radius of curvature  $\rho_{rt} = c^2/a$  which is:

$$\rho_{rt} \simeq \frac{R_{lc}}{2}. \quad (1)$$

The index ‘rt’ is to remind that this is the curvature induced by rotation on electron *trajectory* that is *radial* (or almost radial) in the corotating frame. Near the dipole axis, the curvature radius of dipolar field lines is given by

$$\rho_B \simeq \frac{4}{3} \frac{r}{\sin \theta}, \quad (2)$$

where  $r = |\vec{r}|$  is the radial distance of an emission point and  $\theta$  is the angle between  $\vec{r}$  and the dipole axis.

We look for regions in the trailing part of the polar cap tube, where the rotationally-induced curvature of eq. (1) is cancelled by the curvature of B-field lines. By equating  $\rho_{rt}$  with  $\rho_B$  one can find an equation for the locations of straight portions of the trajectories:

$$\sin \theta_{zc} \simeq \theta_{zc} \simeq \frac{8}{3} \frac{r}{R_{lc}}, \quad (3)$$

<sup>3</sup> Unless specified otherwise, ‘equatorial’ refers to the *rotational* equator.

where the index ‘zc’ stands for ‘zero curvature’. We can see that the locations of the zero-curvature depend on radial distance:  $\theta_{zc} \propto r$ .

In the dipole geometry, magnetic field lines at points with coordinate  $\theta$  are directed at angle  $\theta_k \simeq (3/2)\theta$  with respect to the magnetic axis. Therefore, the phase delay of emission from the zero-curvature regions with respect to the (same altitude) emission along dipole axis is equal to

$$\Delta\phi_{BCW} \simeq \theta_k(\theta_{zc}) \simeq \frac{3}{2} \theta_{zc} \simeq 4 \frac{r}{R_{lc}}. \quad (4)$$

Thus, the locally-straight portions of electron trajectory lag the dipole axis spatially by  $\theta_{zc} \simeq (8/3)r/R_{lc}$ , whereas the tangent-to- $B$  directions of radio waves emitted from these regions lag the direction of waves emitted along the dipole axis by the angle of  $4r/R_{lc}$  radians. Note that until the very end of the derivation there was no need to explicitly refer to the effects of aberration and propagation time delays (APT) that noticeably increase complexity of more general analysis (see Appendix B for the definition of the APT effects). This is because it is the rotational straightening of electron trajectories that is the essence of the effect. As long as one is interested in emission from a fixed altitude, *both* the aberration *and* propagation time effects can be ignored, because the waves emitted along the dipole axis as well as those emitted from the zero-curvature regions are advanced in (absolute) phase by roughly the same magnitude ( $r/R_{lc}$  by aberration and another  $r/R_{lc}$  by propagation time). It is so because in the small angle approximation all the open field lines are basically orthogonal to the corotation velocity (for details see Dyks, Rudak & Harding 2004b, hereafter DRH). The APT effects only have to be included when there are altitude differences, or when one wants to know the magnitude of absolute delays with respect to the “fiducial phase”. This subject will be discussed in detail in the next section.

According to eq. (3), the last open field lines, located near  $\theta_{1o} \simeq (r/R_{lc})^{1/2}$ , have the zero-curvature in IOF at radial distance

$$\frac{r}{R_{lc}} \simeq \frac{9}{64} \simeq 0.14. \quad (5)$$

Note, however, that at this altitude the inaccuracy of our approximation (linear in  $r/R_{lc}$ ) is *not* negligible (it is of the order of  $(r/R_{lc})^{1/2} \sim 40\%$ ).

We can also determine the rotation period  $P = 2\pi/\Omega$  for which the zero curvature occurs at the trailing part of the rim of the polar cap. Since  $\theta_{zc}/\theta_{1o} \simeq (8/3)(r/R_{lc})^{1/2} = 0.0386(r_6/P)^{1/2}$ , with  $r_6 = r/(10^6 \text{ cm})$  and  $P$  in seconds, one obtains:

$$P \simeq 1.49 \cdot 10^{-3} \text{ s } R_6, \quad (6)$$

where  $R_6 = R_{NS}/(10^6 \text{ cm})$  is the neutron star radius. Thus, it happens just in the fastest known millisecond pulsars (J17148–2446 with  $P = 1.396 \text{ ms}$ , Hessels et al. 2006, or B1937+21 with  $P = 1.558 \text{ ms}$ , Backer et al. 1982) that the ‘dipole axis’ is shifted full way to the trailing rim of the polar cap (provided the pulsars have  $\alpha \sim 90^\circ$ , as their interpulses suggest). The effect is illustrated in Fig. 1 of Dyks & Rudak (2002), where a numerically calculated trajectory of photons in the CF (for  $P = 1.5 \text{ ms}$  and  $\alpha = 90^\circ$ ) neatly coincides with the last open field line that emerges from the trailing side of the polar cap. Another consequence is that the efficiency of magnetic pair production in these objects is the

weakest near the trailing side of the polar cap, not at the polar cap center (see Fig. 7 in the last-mentioned paper).

### 3 POLARIZATION ANGLE CURVE

In the absence of the rotational effects the PA as a function of phase is given by:

$$\psi = \tan^{-1} \left[ \frac{\sin \alpha \sin(\phi_{\text{obs}} - \phi_0)}{\cos(\phi_{\text{obs}} - \phi_0) \cos \zeta \sin \alpha - \cos \alpha \sin \zeta} \right] + \psi_{\Omega}, \quad (7)$$

where  $\phi_{\text{obs}}$  is the pulse phase with zero point defined arbitrarily by the observer,  $\phi_0$  is the pulse phase at which the line of sight lies within the  $(\vec{\Omega}, \vec{\mu})$  plane, the constant  $\psi_{\Omega}$  is the position angle of the projection of the pulsar rotation axis on the plane of the sky,  $\alpha$  is the angle between the angular velocity of pulsar rotation  $\vec{\Omega}$  and the dipole magnetic moment  $\vec{\mu}$ , whereas  $\zeta$  is the angle between  $\vec{\Omega}$  and the unit vector of the line of sight  $\hat{n}_{\text{obs}}$ . The sign of the arctan term is for  $\psi$  measured in the observers' conventional way, i.e. *counterclockwise* in the sky (Everett & Weisberg 2001). In this simple geometrical model, the PA is determined purely by projection of magnetic field direction on the sky's plane. Therefore, the azimuth angle  $\phi_{\mu}$  of the dipole axis (measured from the plane which contains an observer and  $\vec{\Omega}$ , see Fig.1) and the pulse phase  $\phi_{\text{obs}}$  are simply related by  $\phi_{\mu} = \phi_{\text{obs}} - \phi_0$ . Let us denote the value of pulse phase at which the center of the PA curve (its inflection point) is observed by  $\phi_{\text{PA}}$  (at this phase  $|d\psi/d\phi_{\text{obs}}|$  has a maximum and  $\psi = \psi_{\Omega}$ ). In the absence of the rotational effects, (and in the case of infinite propagation speed  $c = \infty$ ), the center of the PA curve would be observed at the pulse phase  $\phi_{\text{PA}} = \phi_0$ . Let us use the symbol  $\phi_{\text{prof}}$  to denote the center of the pulse profile defined as the midpoint between the profile's outer edges. As long as the outer boundary of the radio emission region in the CF is symmetric with respect to the  $(\vec{\Omega}, \vec{\mu})$  plane, the center of the pulse profile would be observed at exactly the same phase  $\phi_{\text{prof}} = \phi_0$ .

#### 3.1 Altitude-dependent polarization angle curve

BCW generalized eq. (7) to include rotational effects. By considering the radio emission *from a fixed radial distance*  $r$ , they found that the PA curve is shifted toward later phases by  $\Delta\phi_{\text{BCW}} \approx 4r/R_{\text{lc}}$  with respect to the center of the pulse profile. For this special case of fixed  $r$ , the profile's center is a very convenient reference point from the observational point of view: if measured, the shift can be directly translated into the radial distance  $r/R_{\text{lc}} \approx \Delta\phi_{\text{BCW}}/4$ .<sup>4</sup> For other applications of BCW theory, however, the center of the pulse profile is not a suitable reference point, because the phase at which it occurs ( $\phi_{\text{prof}}$ ) depends on  $r$  itself. For example, the shift (PA center - profile center) does not tell us by how much the PA curve is shifted with respect to the case with the rotational effects ignored. Neither is the profile center helpful if different parts of the profile originate from different altitudes.

<sup>4</sup> To find the phase of inflection point  $\phi_{\text{PA}}$  one can fit the standard PA swing (eq. 7) to the data (as BCW and von Hoensbroech & Xilouris did), because it has nearly the same shape as the equation which includes the rotational effects.

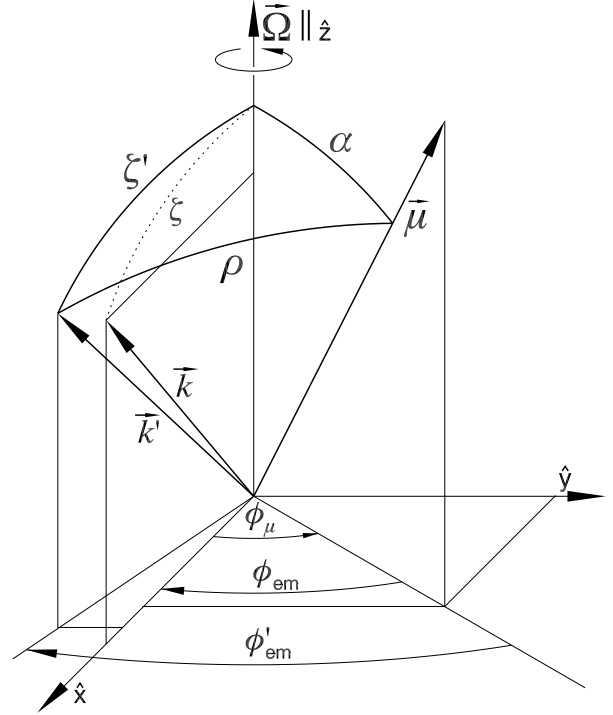


**Figure 1.** Orientation of the CF emission direction  $\vec{k}'$ , IOF emission direction  $\vec{k}$ , and the dipole axis  $\vec{\mu}$  at the moment when radiation emitted at angle  $\rho$  with respect to  $\vec{\mu}$  in the CF becomes directed toward an observer who is located at angle  $\zeta$  from the rotation axis in the  $(\vec{\Omega}, \hat{x})$  plane. The line of sight direction  $\hat{n}_{\text{obs}}$  coincides with  $\vec{k}$ . Up to the order of  $r/R_{\text{lc}}$  the angles  $\zeta$  and  $\zeta'$  can be considered equal. The azimuths  $\phi_{\text{em}}$  and  $\phi'_{\text{em}}$  differ by  $r/R_{\text{lc}}$ . Note that the angles  $\phi_{\text{em}}$  and  $\phi'_{\text{em}}$  are assumed to increase in the opposite direction than  $\phi_{\mu}$ .

A good reference point for measuring altitude-dependent shifts in pulse profiles should be unambiguously associated with the azimuth  $\phi_{\mu}$  of the magnetic dipole axis. This criterion is met by the fiducial phase  $\phi_f$ , defined as follows: it is the pulse phase at which the observer detects a photon that was emitted from the center of the star at the moment when the dipole axis was in the plane containing  $\vec{\Omega}$  and the observer (hereafter  $(\vec{\Omega}, \hat{n}_{\text{obs}})$ -plane). Because  $\phi_{\text{obs}} = \phi_f$  corresponds to  $\phi_{\mu} = 0$  *strictly in the just-described sense*, the fiducial phase  $\phi_f$  plays a similar role as  $\phi_0$  does in eq. 7 (ie. one may consider them identical:  $\phi_f \equiv \phi_0$ ).

The shape of emission region that I consider in this paper is assumed to be axially symmetric around the dipole axis, ie. its radial distance  $r$  can be described as a function of only the angle  $\rho \approx 1.5s(r/R_{\text{lc}})^{1/2}$  between the emission direction in the CF and the dipole axis ( $s = \theta_{\text{surf}}/\theta_{\text{pc}}$  is the footprint parameter of a  $\vec{B}$ -field line on the star surface). Such an *average* form is roughly consistent with the observed shapes of phase-averaged pulse profiles (eg. Johnston et al. 2008; Rankin 1983) but neglects the azimuthal structure (Karastergiou & Johnston 2007; Rankin & Ramachandran 2003). To calculate the PA curve for an arbitrary shape of  $r(\rho)$  one needs an equation for the altitude-dependent PA curve. Equations (16) or (17), (the latter with

$\phi_0 = 3r/R_{lc}$ ), from BCW can be used for this purpose, provided that a transition from ‘ $\Omega t$ ’ to the pulse phase  $\phi_{obs}$  is carefully done.

The equations (16) and (17) of BCW are expressed in the emission time<sup>5</sup> *with the zero point defined in a particular way*:  $t \equiv t_e = 0$  corresponds to the moment when the dipole axis is in the  $(\vec{\Omega}, \hat{n}_{obs})$ -plane. Thus, the emission time in BCW is simply defined as  $t_e = \phi_\mu/\Omega$ , where  $\phi_\mu$  is the azimuth of  $\vec{\mu}$  in the frame with  $\vec{\Omega} \parallel \hat{z}$  and with the observer in the  $(\vec{\Omega}, \hat{x})$  plane (see Fig. 1; this azimuth provides the measure of the emission time). It is very important to discern the emission time (or  $\phi_\mu$ ) from the detection time  $t_d$  (or from pulse phase  $\phi_{obs}$ ) at which the radiation emitted at  $t_e$  is detected. They are related by:

$$t_d = t_e + d/c - \vec{r} \cdot \hat{n}_{obs}/c + \Delta t_{zp}, \quad (8)$$

where  $\hat{n}_{obs}$  is the unit vector pointing towards the observer,  $d$  is the pulsar’s distance and  $\Delta t_{zp}$  takes into account the fact that the observer is allowed to assume arbitrary zero point in the counting of time. The term  $\vec{r} \cdot \hat{n}_{obs}/c$  (‘propagation time advance’) takes into account the fact that the source located at  $\vec{r}$  is closer to the observer than the center of the neutron star. The same can be expressed in terms of angles:

$$\phi_{obs} = \phi_\mu + \Omega d/c - \Omega \vec{r} \cdot \hat{n}_{obs}/c + \Delta \phi_{zp}, \quad (9)$$

where  $\phi_{obs} = \Omega t_d$ , and  $\Delta \phi_{zp}$  takes into account the fact that the observer can assign phase zero to the pulse profile in an arbitrary way. The pulsar distance  $d$  and the zero point difference  $\Delta \phi_{zp}$  can be replaced in this equation with the fiducial phase. The definition of  $\phi_f$ , as articulated above, is

$$\phi_f = \phi_{obs} (\phi_\mu=0, r=0) = \Omega d/c + \Delta \phi_{zp} \quad (10)$$

(from eq. 9), which can be inserted back into (9) to obtain:

$$\phi_{obs} = \phi_\mu - \Omega \vec{r} \cdot \hat{n}_{obs}/c + \phi_f \approx \phi_\mu - r/R_{lc} + \phi_f, \quad (11)$$

where on the right hand side I make the small-angle approximation:  $\vec{r} \cdot \hat{n}_{obs} \approx r$  and use  $\Omega/c = 1/R_{lc}$ . Remembering that  $\phi_\mu = \Omega t_e$  we get:

$$\Omega t_e = \phi_{obs} - \phi_f + r/R_{lc} \quad (12)$$

which should be used in equations (16) and (17) of BCW in place of ‘ $\Omega t$ ’ (the common practice of replacing  $\Omega t$  in eqs. (16) and (17) of BCW with  $\phi_{obs}$  results in PA curves that lag the fiducial phase by  $3r/R_{lc}$  instead of the actual  $2r/R_{lc}$ ; therefore they underestimate  $r$  by a factor of 1.5.)

Thus, the equation for the altitude-dependent PA curve reads:

$$\psi_r \approx \tan^{-1} \left[ \frac{3(r/R_{lc}) \sin \zeta - \sin \alpha \sin(\phi_{obs} - \phi_f + r/R_{lc})}{\sin \beta + \sin \alpha \cos \zeta (1 - \cos[\phi_{obs} - \phi_f + r/R_{lc}])} \right] + \psi_\Omega, \quad (13)$$

where  $\beta = \zeta - \alpha$  is the observer’s ‘impact’ angle. The equation was obtained directly from eq. (16) in BCW (in addition to the use of  $\Omega t = \phi_{obs} - \phi_f + r/R_{lc}$  I have changed the BCW’s sign of the arctan term to agree with the observers’ convention).

<sup>5</sup> The emission time refers to a Lorentz frame in which the pulsar’s center of mass is at rest. Note that BCW use two different symbols to denote it ( $t$  as well as  $t_e$ ).

The same approach may be applied to eq. (17) of BCW (with  $\phi_0 = 3r/R_{lc}$ ) to get:

$$\psi_r \approx \tan^{-1} \left[ \frac{-\sin \alpha \sin(\phi_{obs} - \phi_f - 2r/R_{lc})}{\sin \beta + [1 - \cos(\phi_{obs} - \phi_f - 2r/R_{lc})] \cos \zeta \sin \alpha} \right] + \frac{10}{3} \frac{r}{R_{lc}} \cos \alpha + \psi_\Omega, \quad (14)$$

which is equivalent to (13) within the accuracy of the BCW method, ie. up to the order of  $r/R_{lc}$ . The manually-added term  $(10/3)(r/R_{lc}) \cos(\alpha)$  represents the vertical shift of the PA found by HA (the shift given in HA refers to the clockwise definition of PA, and, therefore, has opposite sign). For the polar-current flow that is close to the Goldreich-Julian value, this term is cancelled and can be neglected in eqs. (14) and (15). In such a case, however, the current-induced shift of PA must also be subtracted from eq. (13) for consistency (see Sect. 4.2 below).

Yet another, most direct method to derive the equation for the altitude-dependent PA curve is the following. The center of the pulse profile precedes in phase the center of the PA swing by  $4r/R_{lc}$ , ie.  $\phi_{PA} \approx \phi_{prof} + 4r/R_{lc}$ . The profile center itself precedes the fiducial phase  $\phi_f$  by  $2r/R_{lc}$  (one  $r/R_{lc}$  for the aberration and another  $r/R_{lc}$  for the propagation time, see eg. DRH for details). Therefore, the center of the PA curve lags the fiducial phase  $\phi_f$  by  $4r/R_{lc} - 2r/R_{lc} = 2r/R_{lc}$  and at any phase  $\phi_{obs}$  the position angle  $\psi_r$  which includes the rotational effects is equal to the ‘nonrelativistic’ PA (given by eq. 7) taken at the earlier phase  $\phi_{obs} - 2r/R_{lc}$ . Thus,  $\psi_r(\phi_{obs}) = \psi(\phi_{obs} - 2r/R_{lc})$ :

$$\psi_r \approx \tan^{-1} \left[ \frac{\sin \alpha \sin(\phi_{obs} - \phi_f - 2r/R_{lc})}{\cos(\phi_{obs} - \phi_f - 2r/R_{lc}) \cos \zeta \sin \alpha - \cos \alpha \sin \zeta} \right] + \frac{10}{3} \frac{r}{R_{lc}} \cos \alpha + \psi_\Omega \quad (15)$$

This equation was simply obtained by replacing  $\phi_{obs}$  in eq. (7) with  $\phi_{obs} - 2r/R_{lc}$  and by replacing  $\phi_0$  with  $\phi_f$ . Simple trigonometry shows that it is equivalent to eq. (14).

In the limit of  $r \ll 10^{-2} R_{lc}$  all eqs. (13) – (15) reduce to eq. (7) and the centers of PA the curve, the pulse profile, and the fiducial phase coincide. In eqs. (13) – (15) the radiation electric field  $\vec{E}_w$  is assumed to be along, rather than orthogonal to, the direction of electron acceleration  $\vec{a}$  (in eq. 7  $\vec{E}_w$  is assumed to be along the magnetic field  $\vec{B}$ , or at least in the plane of a  $\vec{B}$ -field line). For the case  $\vec{E}_w \perp \vec{a}$  (or for  $\vec{E}_w \perp \vec{B}$ ), the value of PA given by eqs. (7), (13), (14), and (15) may need to be increased by  $90^\circ$  (as in the case of the Vela pulsar, Lai et al. 2001, Radhakrishnan & Deshpande 2001). Obviously, if the projection of the rotation axis at the plane of the sky is unknown the terms  $\psi_\Omega$  in eq. (7) and (13) – (15) must be considered free parameters to be determined from the fit to the data. If  $r$  is independent of pulse phase and we are not interested in the value of  $\psi_\Omega$ , the term  $(10/3)(r/R_{lc}) \cos \alpha$  can be merged with  $\psi_\Omega$  into a single fitting parameter.

Eq. (15) depends only on the term  $-\phi_f - 2r/R_{lc}$  which makes it difficult to separate  $\phi_f$  from  $r$ . A special case when it is possible is when  $r$  does not change across the pulse profile. In such a case the center of the PA curve (the inflection point) is located at the phase

$$\phi_{PA} \approx \phi_f + 2r/R_{lc}. \quad (16)$$

The center of the pulse profile is then located at

$$\phi_{\text{prof}} \approx \phi_f - 2r/R_{\text{lc}} \quad (17)$$

so that the shift of the PA with respect to the profile is  $\phi_{\text{PA}} - \phi_{\text{prof}} \approx 4r/R_{\text{lc}}$ . Then (i.e. for  $r = \text{const}$ ) eqs. (16) and (17) tell us that

$$\phi_f = (\phi_{\text{prof}} + \phi_{\text{PA}})/2, \quad (18)$$

ie.  $\phi_f$  is half way between the center of the pulse profile and the center of the PA curve (Fig. 2). If the nature and the quality of the data allow us to determine  $\phi_{\text{prof}}$  and  $\phi_{\text{PA}}$ , the value of  $\phi_f$  can be calculated from (18) under the assumption that  $r = \text{const}$ . In this specific case  $\phi_{\text{PA}}$  can be determined by fitting the *nonrelativistic* PA curve (eq. 7) to the observed data.

### 3.2 Relation between the radial distance of radio emission and the pulse phase at which it is detected

In the case of emission altitude that changes gradually with pulse phase  $\phi_{\text{obs}}$ , the eqs. (13) – (15) must be supplemented by an analytical equation for  $r = r(\phi_{\text{obs}})$  to be useful.

If the distribution of emissivity in the CF frame is symmetrical with respect to the dipole axis, the radial distance of the radio emission  $r$  is a function of only the angle  $\rho$  between the emission direction in the CF and the dipole axis. Let us assume that the emission region can be described by a simple function  $r(\rho)$  which can be inverted<sup>6</sup> into  $\rho(r)$ .

Fig. 1 shows relative orientations of the dipole axis  $\mu$ , and the CF-emission direction  $\vec{k}'$  at the moment when the radiation is directed towards the observer. In the IOF it propagates along  $\vec{k} \parallel \hat{n}_{\text{obs}}$ .

The radiation from some point at radial distance  $r$  is directed towards the observer only when  $\vec{\mu}$  is rotated by an appropriate angle  $\phi_\mu = \phi_{\text{em}} = \Omega t_{\text{em}}$ . Because the aberration advances the radiation by  $r/R_{\text{lc}}$  in phase, the angle  $\phi_{\text{em}}$  is smaller by  $r/R_{\text{lc}}$  than the angle  $\phi'_{\text{em}}$  by which the dipole would need to be rotated in the absence of the aberration to become aligned with the line of sight (see Fig. 1):

$$\phi'_{\text{em}} \simeq \phi_{\text{em}} + r/R_{\text{lc}} = \Omega t_{\text{em}} + r/R_{\text{lc}}. \quad (19)$$

From (12) and (19) we learn that the radiation is shifted toward earlier phases by  $2r/R_{\text{lc}}$  with respect to  $\phi_f$  and is detected at the phase:

$$\phi_{\text{obs}} \simeq \phi_f + \phi'_{\text{em}} - 2r/R_{\text{lc}}. \quad (20)$$

By substituting  $\phi_{\text{obs}}$  in eq. (15) by the above formula, and using  $\phi'_{\text{em}} \simeq \phi_{\text{em}} + r/R_{\text{lc}}$ , as well as  $\phi_{\text{em}} = \Omega t_{\text{em}}$  one can easily verify that eq. (15) is equivalent with eq. (17) in BCW.

Unlike  $\phi_{\text{em}}$  (see Fig. 1), the azimuth  $\phi'_{\text{em}}$  of the non-aberrated emission direction  $\vec{k}'$  is associated with the angle  $\rho$  between  $\vec{\mu}$  and  $\vec{k}'$  through:

$$\cos[\rho(r)] = \cos \phi'_{\text{em}} \sin \alpha \sin \zeta' + \cos \alpha \cos \zeta', \quad (21)$$

<sup>6</sup> If more than one value of  $r$  correspond to the same value of  $\rho$  (ie. if there are several layers of emission located above each other) one can separate  $r(\rho)$  into a few functions  $\rho$ , each of which is reversible. Since emission from different layers can be observed simultaneously, the Stokes parameters must be used as eg. in KD83 or Mitra & Seiradakis (2004).

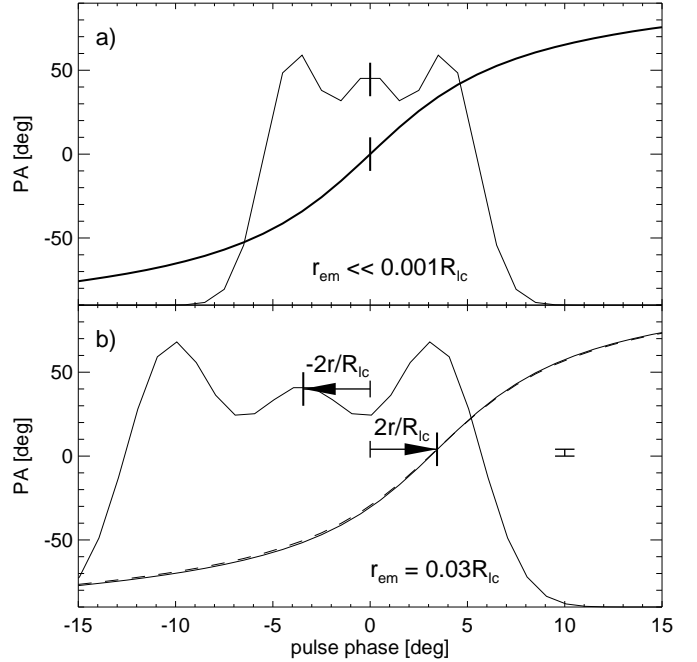


**Figure 2.** Influence of increased emission altitude on the observed PA curve. Panel **a**) shows the RC69 case of negligible emission altitude. In **b**) the emission altitude has been risen up to  $0.03R_{\text{lc}}$ . As a result, both the intensity profile and the PA curve move in opposite directions from the fiducial phase by the same angle of  $2r/R_{\text{lc}}$  rad. In both panels pulse phase zero is the fiducial phase (‘dipole axis phase’). In BCW, the only figure that has the fiducial phase at  $\phi_{\text{obs}} = 0$  is their fig. 3. The apparently small bar at  $\phi_{\text{obs}} = 10^\circ$  shows the vertical upward shift of the PA curve by  $(10/3)(r/R_{\text{lc}}) \cos \alpha$ . The solid PA curve in **b**) presents the approximate equation of BCW (eq. 13 in this paper). The dashed line is just the appropriately shifted RVM curve (eq. 14). In **a**) they coincide. In the figure  $\alpha = 45^\circ$  and  $\zeta = 41.3^\circ$ . In all figures  $\psi_\Omega = 0$ .

which is a direct form of the spherical trigonometry cosine theorem applied for the triangle  $(\vec{\Omega}, \vec{k}', \vec{\mu})$ . Calculating  $\phi'_{\text{em}}$  from (21) and inserting into eq. (20) gives

$$\phi_{\text{obs}}(r) \simeq \pm \cos^{-1} \left( \frac{\cos(\rho(r)) - \cos \alpha \cos \zeta}{\sin \alpha \sin \zeta} \right) + \phi_f - 2 \frac{r}{R_{\text{lc}}}, \quad (22)$$

where we ignored the insignificant difference between  $\zeta$  and  $\zeta'$ . The ‘+’ sign at the arccos term corresponds to the trailing whereas the ‘-’ sign to the leading part of the open field line region.

Since the argument of the function arccos in eq. (22) does not have to be small (e.g. for small dipole inclination  $\alpha$  the profile width can reach several tens of degrees), the equation in general cannot be inverted to obtain a simple analytical formula for  $r(\phi_{\text{obs}})$ . To use eq. (15) for phase-dependent  $r$ , the latter needs to be determined from (22) numerically.

### 3.3 Numerical example

Eq. (22) is useful for a quick examination of the shape of PA curves for a variety of emission regions, ie. for various functions  $r(\rho)$ . A convenient way of doing this is to define a dense table of angles  $\rho_i$ , and calculate the corresponding

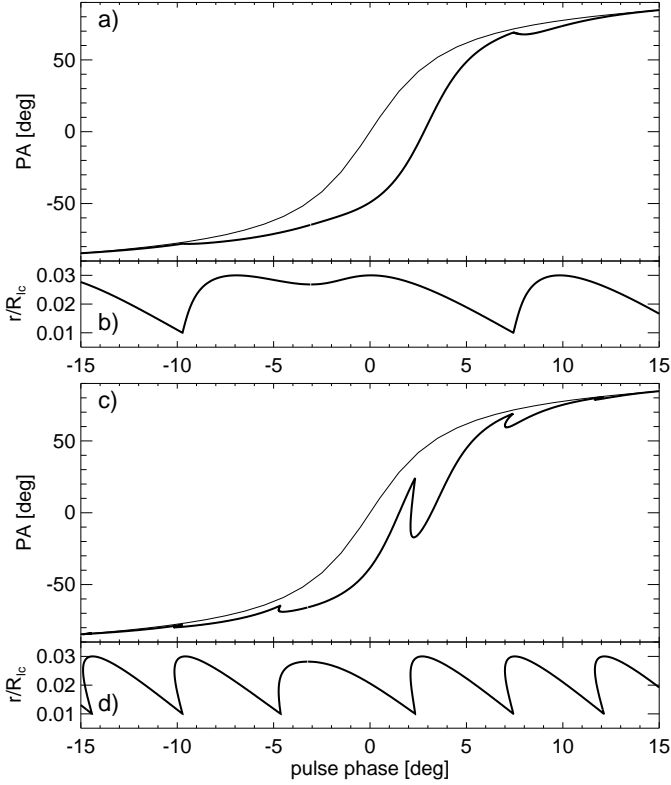


**Figure 3.** Altitude-dependent PA curves (thick lines in **a** and **c**) calculated by using eqs. (22) and (13) for the emission region of eq. (23) with  $a_0 = 2^\circ$  (top) and  $a_0 = 1^\circ$  (bottom). The thin line shows the standard RVM curve for reference. Panels **b** and **d** show the corresponding radial distances in units of  $R_{lc}$ . Phase  $\phi_{\text{obs}} = 0$  is the fiducial phase and I used  $\alpha = 45^\circ$  and  $\zeta = 43^\circ$  in the figure.

vector of  $r_i(\rho_i)$  for some chosen function  $r(\rho)$  (or vice versa: to define  $r_i$  and calculate  $\rho_i(r_i)$  for arbitrarily selected  $\rho(r)$ ). These are next used in eq. (22) to calculate the table of the corresponding values of  $\phi_{\text{obs},i}$ . The tables  $r_i$ , and  $\phi_{\text{obs},i}$  can then be directly used in eq. (13) (or 25) to calculate the shape of the PA curve  $\psi(\phi_{\text{obs}}, r)$ .

Fig. 3 presents an example of such procedure performed for the emission region given by:

$$\frac{r}{R_{lc}} = 0.01 + 0.02 \left| \sin \left( \frac{\rho}{a_0} \right) \right|, \quad (23)$$

where the constant  $a_0 = 2^\circ$  was used in panels a and b, whereas  $a_0 = 1^\circ$  in c and d (this somewhat strange shape was chosen to make the distortions of the PA curves easily noticeable by eye). The curves  $r(\phi_{\text{obs}})$  (as given by eq. 22) are shown in panels b and d. One can see the characteristic skewing of the  $r(\phi_{\text{obs}})$  function toward early phases, which is caused by the APT effects. In panel d, the radial distance  $r$  increases with phase so fast that the radiation from the upper parts of the emission region overlaps in phase with radiation emitted at lower altitudes. The corresponding PA curve (panel c) is not a mathematical function of phase (there are a few regions with three values of PA referring to the same  $\phi_{\text{obs}}$ ). To look normal it needs to be cut into pieces and Stokes-summed (for details see Mitra & Seiradakis 2004; KD83).

## 4 LIMITATIONS ON THE VALIDITY AND APPLICABILITY OF THE LINEAR THEORY

The equations of Sect. 3 refer to phase shifts that are usually tiny and can be easily affected by several interfering effects discussed in this section. Moreover, the accuracy of the analytical results of previous sections is limited by their inherent error of  $(r/R_{lc})^{1/2}$ . The validity of the analytical theory is therefore severely limited: on one hand by the too small magnitudes of the phase shifts (too small to be reliably measured, or to be unaffected by the disturbing effects); on the other hand by the poor accuracy of the theory at larger  $r$ . The following subsections are to show that it makes practically no sense to apply the theory for  $r \gtrsim 0.1R_{lc}$  ( $\Delta\phi_{\text{obs}} \gtrsim 10^\circ - 20^\circ$ ).

### 4.1 Asymmetry of the open field line region caused by rotational distortions of the magnetic dipole (sweepback)

The strict symmetry of the open volume with respect to the  $(\vec{\Omega}, \vec{\mu})$ -plane is unlikely, and it has been shown (Dyks & Harding 2004, hereafter DH04) that even very small effects (that at low altitudes are of high order in  $r/R_{lc}$ ) can easily introduce large asymmetry. Here I discuss the rotational deformations of the vacuum dipole (DH04; Shitov 1983, Deutsch 1955), because they are easy to analyze (thanks to the existing analytical formulae) and they seem to be qualitatively similar to those obtained in recent plasma-loaded simulations (eg. Spitkovsky 2008). As we show in detail in DH04, in the lowest order (of  $(r/R_{lc})^2$ , which is already higher than the  $r/R_{lc}$  accuracy of equations in the preceding sections) the rotational sweepback does not introduce any asymmetry to the  $B$ -field direction. The asymmetric change of  $\vec{B}$ -field direction is of the order of  $(r/R_{lc})^3$  at low altitudes (completely negligible *there*). Despite this, a very strong asymmetry of the open volume (of magnitude  $\sim (r/R_{lc})^{1/2}$ ) is generated by the sweepback. This is because the low-altitude outer boundary of the open volume is determined by the geometry of  $\vec{B}$  at the *light cylinder*, where the sweepback becomes a strong effect (first order, in the sense that there we have  $(r/R_{lc})^a \sim 1$ , regardless of  $a$ ). This strong distortion is traced back towards low altitudes through the continuity of magnetic field lines, and results in strong (much stronger than  $(r/R_{lc})^3$ ) asymmetry of the open volume.

This effect can be taken into account by replacing the delay-radius relation (eq. 4) with the ‘misalignment’ formula of DH04:

$$\Delta\phi \simeq 4 \frac{r}{R_{lc}} - F \left( \frac{r}{R_{lc}} \right)^{1/2}, \quad (24)$$

where  $F$  depends on  $\alpha$  and  $\zeta$  and has typically the magnitude of  $\sim 0.2$ . Eq. (24) differs from the original delay-radius relation only in that it takes into account the azimuthal asymmetry of the outer boundary of the open field line region. However, I do not refer to eq. (24) with the name ‘delay-radius’ relation because the shift of position angle curve does not have to be the positive delay anymore – it can now *slightly* precede the profile midpoint, see DH04 for more details.

Those, who believe that the *rotating* vacuum dipole is a

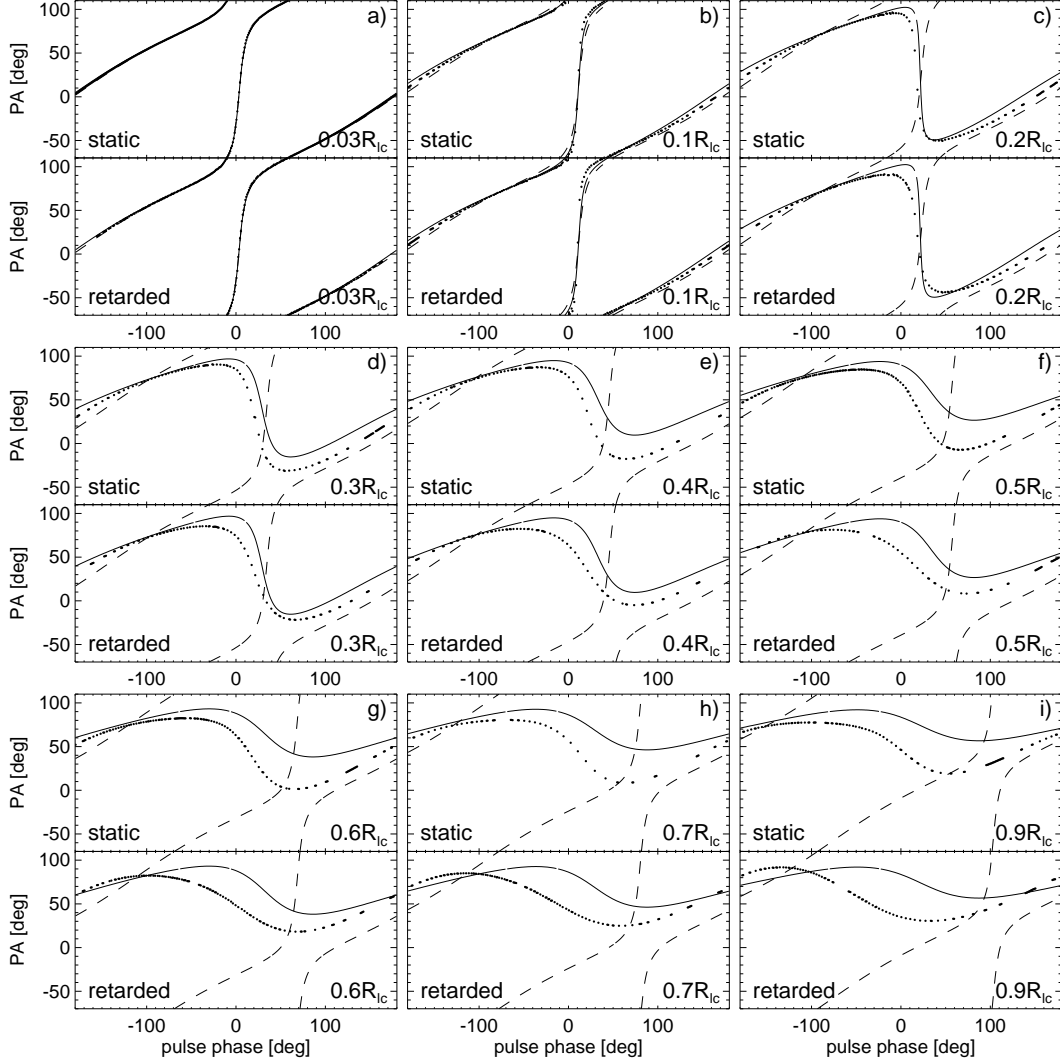


**Figure 4.** Variations of polarization angle curve due to increasing emission altitude, marked in the bottom right corners of each panel. The dots, often merging into a thick solid line, present exact numerical solution. The thin solid line presents the equation (13). The dashed line is for eqs. (14) and/or (15). For each altitude the numerical curve is shown for both the static-shape dipole (letter-marked panels) and the rotationally-distorted vacuum dipole (below the static case). The figure was calculated for  $\alpha = 45^\circ$ ,  $\zeta = 41.3^\circ$ ,  $\phi_f = 0$ , and  $\psi_\Omega = 0$ .

better approximation of the real  $\vec{B}$  than the static vacuum dipole should use eq. (24) instead of the original delay-radius relation of BCW. What may be most reasonable is to use both the eq. (24) and (4) as the lower and upper limit for  $r$ , respectively.

#### 4.2 Current-induced distortions of magnetic field

The magnitude of the current-induced distortions of magnetic field can be easily estimated with a simplification of Ampere's law  $\nabla \times \vec{B} = c^{-1}(4\pi\vec{J} + \partial\vec{E}/\partial t)$  into the crude form of  $\Delta B/L \sim J/c$ , where  $\Delta B$  is the magnetic field generated by the current density  $J$ , and  $L$  is the characteristic scale. For longitudinal polar currents of the Goldreich-Julian (GJ) magnitude we have  $J \sim J_{GJ} \sim \rho_{GJ}c$ , where  $\rho_{GJ} \simeq \Omega B/(2\pi c) \sim B/R_{lc}$  is the GJ density, whereas the transverse scale  $L \simeq r\theta_{lo} \simeq r(r/R_{lc})^{1/2}$  corresponds to the open field line region. The distortions of  $B$  are therefore of

the order of  $(\Delta B/B)_{\text{polar}} \sim (r/R_{lc})^{3/2}$ . For toroidal currents (due to the corotation of  $\rho_{GJ}$ ) we have  $J \sim \rho_{GJ}v_{\text{rot}}$  where  $v_{\text{rot}} = \Omega r = cr/R_{lc}$  is the local corotation velocity, and  $L \sim r$ . This results in smaller distortions of  $(\Delta B/B)_{\text{trdl}} \sim (r/R_{lc})^2$ .

HA find that the polar currents shift the PA curve downward by  $\Delta\psi_J = -(10/3)(r/R_{lc})(J/J_{GJ})\cos\alpha$ . A spectacular way of estimating the current density has recently become possible thanks to the observations of part-time pulsars (Kramer et al. 2006) and suggests that  $J \sim J_{GJ}$  during the 'on' phase of pulsar emission.

The simplest way to include the effects of current in the approximate eqs. (13) – (15) is to subtract the term  $(10/3)(r/R_{lc})(J/J_{GJ})\cos\alpha$  with  $J/J_{GJ} = 1$  from their right-hand sides, to obtain:

$$\psi_r \approx \tan^{-1} \left[ \frac{3(r/R_{lc})\sin\zeta - \sin\alpha\sin(\phi_{\text{obs}} - \phi_f + r/R_{lc})}{\sin\beta + \sin\alpha\cos\zeta(1 - \cos[\phi_{\text{obs}} - \phi_f + r/R_{lc}])} \right] +$$

$$- \frac{10}{3} \frac{r}{R_{\text{lc}}} \cos \alpha \left( \times \frac{J}{J_{\text{GJ}}} \right) + \psi_{\Omega} \quad (25)$$

for the BCW formula of eq. (13), and

$$\psi_r \approx \tan^{-1} \left[ \frac{\sin \alpha \sin(\phi_{\text{obs}} - \phi_f - 2r/R_{\text{lc}})}{\cos(\phi_{\text{obs}} - \phi_f - 2r/R_{\text{lc}}) \cos \zeta \sin \alpha - \cos \alpha \sin \zeta} \right] + \psi_{\Omega} \quad (26)$$

for the ‘shifted RVM’ curve of eqs. (14) and (15).

### 4.3 Shapiro delay

To make things possibly simple, the importance of general relativistic time delays has been neglected so far. These should not affect the delay-radius relation, because it refers only to a single  $r$ , and is insensitive to any time delays (whether gravitational or flat spacetime). They do affect, however, all formulae which refer to altitude differences (as do all the equations that explicitly involve both  $r$  and  $\phi_f$ ). Let us then use the Schwarzschild metric to learn when the Shapiro delay cannot be neglected. The time for a ray to travel radially in the gravitational field from some  $r_{\text{min}}$  up to  $r_{\text{max}}$  is

$$\Delta t_{\text{Schwzld}} = \int_{r_{\text{min}}}^{r_{\text{max}}} \frac{dr}{c(1 - r_g/r)}, \quad (27)$$

where  $r_g = 2GM_{\text{NS}}/c^2$ . Instead of that, our flat spacetime formulae assume the time is the Römer delay  $(r_{\text{max}} - r_{\text{min}})/c$ , so they miss the fact that the low altitude emission components (emitted at  $r_{\text{min}}$ ) are additionally Shapiro-delayed by  $\Delta t_{\text{Sh}} = \Delta t_{\text{Schwzld}} - (r_{\text{max}} - r_{\text{min}})/c$  with respect to the high-altitude emission components emitted at  $r_{\text{max}}$ .

In the case of millisecond pulsars (MPs) this effect can become easily measurable: for  $r_{\text{min}} = 10^6$  cm,  $r_{\text{max}} = 0.2R_{\text{lc}}$ , and  $P = 3$  ms, we obtain  $\Delta t_{\text{Sh}} = 2 \cdot 10^{-5}$  s which corresponds to the phase shift of  $2.48^\circ$ . For the same  $r_{\text{min}}$  and  $r_{\text{max}}/R_{\text{lc}}$  but for  $P = 1.5$  ms the phase shift is  $1.95^\circ$ . It becomes slightly smaller because for the fixed  $r_{\text{max}}/R_{\text{lc}} = 0.2$  the altitude difference decreased (for  $P = 3$  ms  $R_{\text{lc}}$  is  $14.3 \cdot 10^6$  cm, whereas for  $P = 1.5$  s it is twice smaller). Note that in the estimate I take  $r_{\text{max}} = 0.2R_{\text{lc}}$  as a blind guess of the upper limit for radio emission regions in millisecond pulsars. This is simply because the known estimates or radio emission altitudes for classical pulsars (a few tens of  $R_{\text{NS}}$ , DRH; Gupta & Gangadhara 2003; Kijak & Gil 1997) would locate the emission region beyond the light cylinder in the millisecond pulsars. If one takes  $r_{\text{max}} = R_{\text{lc}}$ , the gravitational phase shifts become  $5.44^\circ$  and  $8.41^\circ$  for  $P = 3$  and 1.5 ms, respectively. Thus, the equations that rely on altitude differences cannot be reliably applied to fast millisecond pulsars (in particular, it is not safe to use eq. (17) to determine emission altitudes from the core-cone shift). Another reason for not applying the approximate theory to the MPs is that it is very inaccurate for altitude differences of  $\Delta r \gtrsim 0.1R_{\text{lc}}$ , which are likely in fast MPs even if the radio emission extends radially by only one  $R_{\text{NS}}$ . To calculate the phase shifts for MPs even more accurately, one would have to use the metric for a fast rotating neutron star (eg. Braje et al. 2000; Gonthier & Harding 1994; see also D’Angelo & Rafikov (2007) for a detailed description of how the altitude differences affect timing).

In the case of classical pulsars (with  $P \sim 1$  s and  $r_{\text{max}} \simeq 50R_{\text{NS}}$ ), the Shapiro delays can be safely ignored, because they comprise a tiny fraction of the (now longer) rotation period. The phase shifts typically have a few hundredths of a degree.

### 4.4 Limited accuracy of the lowest-order theory

The relativistic phase shifts are of the order of  $r/R_{\text{lc}}$ , whereas the lowest-order terms that have been neglected in derivation of eqs. (13) – (15) have magnitude of  $\sim (r/R_{\text{lc}})^{3/2}$ . This means that the analytical approximations for the polarization angle have a fractional error of  $100(r/R_{\text{lc}})^{1/2}$  percent, which is as large as 30% already at  $0.1R_{\text{lc}}$ . The approximate equations (13) – (15) are compared to the exact numerical PA curves in Fig. 4. The numerical PA curves were calculated for fixed emission altitudes (shown in bottom right corners) and only involve the kinematic effects of corotation (the method of calculation is described in sect. 2 of Dyks et al. 2004a). It is seen that for any  $r \gtrsim 0.1R_{\text{lc}}$  there are considerable differences between the exact result (dots) and the approximate formulae. One can also see that at large altitudes the approximate formula of BCW (eq. 13, thin solid lines) performs much better than the appropriately shifted classic equation of Komesaroff (eqs. 14 and 15, dashed lines).

An interesting effect seen in Fig. 4 is that for large altitudes the numerical PA curves strongly tend to assume the distorted-sine-like (‘equatorward’) shape, in spite of that the figure is for the poleward viewing geometry ( $\alpha = 45^\circ$ ,  $\zeta = 41.3^\circ$ ). The range of  $\zeta$  with the equatorward PA shape is not limited to the range  $(\alpha, \pi - \alpha)$  and is instead increasing with altitude. For the specific case shown in Fig. 4 the numerically determined range of the equatorward PA curve is  $(43^\circ, \pi - 43^\circ)$  for  $r = 0.1R_{\text{lc}}$ , and  $(38.5^\circ, \pi - 38.5^\circ)$  for  $r = 0.2R_{\text{lc}}$  (with numerically-limited accuracy of  $\sim 0.5^\circ$ ). The BCW equation for the PA (eq. 13) does reproduce this behaviour (to some limited degree), but the fixed-shape PA curve of the ‘relativistically shifted’ RC69 model (eq. 14 or 15) fails to do this, which results in the large disagreement already visible in panel c of Fig. 4 (for  $r = 0.2R_{\text{lc}}$ ).

Another interesting effect in Fig. 4 can be seen if one compares PA curves of the static-shape dipole to the distorted (‘retarded’) dipole case. At large altitudes ( $r \gtrsim 0.7R_{\text{lc}}$ ) the sine-like PA curves for the distorted dipole (Fig. 4h,i) move leftward (toward earlier phases) and have their steepest gradient point shifted leftward with respect to the fiducial phase (opposite than expected from the BCW theory). This effect is caused by backward bending of magnetic field lines (the sweepback) which shifts the spatial location of ‘magnetic axis’ (here I mean a locally straight  $\vec{B}$ -field line at a given  $r$ ) forward, into the leading part of pulsar magnetosphere. At large  $r$  this effect seems to dominate the straightening of electron trajectories.

The distorted-sine shape of the high-altitude PA curves, with the steepest gradient point well ahead of the ‘dipole-axis’ phase, bears close resemblance to the unusual PA curve of the pedestal radio emission of B1929+10, where the steepest gradient *precedes* the main pulse by as much as  $18^\circ$  (Rankin & Rathnasree 1997; Everett & Weisberg 2001). This interpretation would imply that the pedestal radio emission



originates from  $r \sim 0.7R_{lc}$ . However, below I also mention other possible interpretations of this effect.

#### 4.5 Limitations due to the specific radio emission mechanism assumed in the theory

The radio emission mechanism assumed in the BCW theory is the curvature radiation caused by the ‘macroscopic’ acceleration due to the curvature of magnetic field lines. The acceleration is small enough that the corotation can modify it to produce the delay-radius relation of eq. (4). The operation of the curvature radiation in pulsar magnetosphere is, however, still a matter of debate (eg. Luo & Melrose 1992; Kunzl et al. 1998).

The other emission processes (eg. the direct or inverse-Compton-scattered plasma emission, or the synchrotron emission) typically involve much larger accelerations due to microscopic motions, that are unlikely to be noticeably affected by the corotation (eg. the acceleration due to gyration exceeds the macroscopic acceleration due to the corotation by a factor  $\omega_B/\Omega \sim 10^8 [B/(10^6\text{G})](\gamma/10^3)^{-1}$ , where  $\omega_B$  is the gyration frequency, Takata et al. 2007).

It is then tempting to speculate that the PA curves for such emission processes would not be delayed by the BCW effect. But the aberration and propagation time effects would still be there, and would shift the PA curve by  $2r/R_{lc}$  toward *earlier* phase than the main pulse. This may be a mechanism responsible for the leftward shift of the pedestal PA in B1929+10. In Dyks, Rudak & Rankin (2007; hereafter DRR) we provide other arguments for non-curvature origin of the pedestal emission. The main pulse emission, on the other hand, does not exhibit the abnormal shift which makes it more consistent with the curvature radiation.

### 5 ANTI-BCW SHIFTS OF PA CURVE

The best examples of this phenomenon are provided by the pedestal radio emission of B1929+10 and the weak bridge of radio emission that connects the main pulse and interpulse of B0950+08. The PA curves of these extended components (fitted *without* the part under the main pulse, see Everett & Weisberg 2001) have their steepest gradient points well on the leading side of the main pulse. So far the following mechanisms have been considered for this effect:

(i) The high-altitude curvature emission from roughly fixed altitude (Sect. 4.4 in this paper and Fig. 4h,i). This probably cannot explain the case of B0950+08, for which the PA curve has the poleward shape.

(ii) Radio emission mechanisms different than curvature radiation (sect. 4.5). Possibly consistent with the parallel-ICS interpretation of double notches (DRR).

(iii) Inward curvature radiation. Proposed simply as an inverted version of the BCW effect (Dyks et al. 2005). The ‘pulsar shadow’ model of double notches, that has led to this interpretation, has been superceded by the model described in DRR.

(iv) Yet another interpretation can be devised using the ‘limiting polarization radius’ idea: polarization of the radiation propagating through the inner (dense) regions of the pulsar magnetosphere can follow the *local* direction of

magnetic field (eg. Cheng & Ruderman 1979; Melrose 1979; Barnard 1986) until the radiation reaches the polarization-limiting radius  $r_{pol}$ . The plasma-density-dependent estimates of  $r_{pol}$  are highly uncertain (eg. Lyubarsky 2002) but it should be significantly larger than the radial distance of the emission region.

High-up in the pulsar magnetosphere the polar beam of radio emission, emitted at low altitudes, propagates through the *trailing* part of open field line region (see fig. 1 in Dyks & Rudak 2002, or fig. 1 in Lyubarsky 2002). Therefore, the polarization imprinted in the beam at  $r_{pol}$  reflects the trailing part of the polarization curve, with the steepest gradient point shifted considerably towards early phases. The same mechanism was proposed by Lyubarsky (2002) to explain the shallowness of PA curves observed in millisecond pulsars (Xilouris et al. 1998). Let me emphasize that the parallel-ICS model of pedestal emission mentioned in point (ii) above, actually *necessitates* this propagation-induced linear polarization. Otherwise the observed polarization degree would be very low due to the convolution of many micro-beams contributing to the line of sight.

### 6 DISCUSSION – ABERRATION OR NOT?

It is shown in Sect. 2 that the magnitude of the shift given by the delay-radius relation has nothing to do with the aberration (understood as the normal beaming effect). On the other hand, Hibschan & Arons mention a phase shift of  $3r/R_{lc}$  (their eq. 4) and claim that it is just the aberration (“simple beaming”) that is responsible for the remaining  $r/R_{lc}$  part of the total delay. Do we have a contradiction here?

Not really, though the wording of HA can easily be misunderstood. Both in the BCW and HA, the delay-radius relation is derived as a difference of two moments of emission: 1) the moment when the radiation bearing the steepest-gradient PA is directed to the observer (this happens at  $\Omega t_e = 3r/R_{lc}$ ) and 2) an earlier moment when the radiation in the middle of the profile (emitted in the  $(\vec{\Omega}, \vec{\mu})$ -plane in the CF) becomes directed toward the observer. HA explicitly notice that the latter does *not* take place at the moment  $t_e = 0$ , when the dipole axis is in the  $\vec{\Omega}$ -observer plane: instead, because of the aberration it happens at  $\Omega t_e = -r/R_{lc}$  (see Fig. 1 and eq. 19 with  $\phi'_{em} = 0$ ). The key point that is not mentioned in their description, however, is that the moment  $\Omega t_e = 3r/R_{lc}$  at which the steepest gradient radiation is directed toward the observer has already been also advanced in time by the same aberration angle of  $r/R_{lc}$ . Thus, *the aberration, understood as the normal beaming effect, works identically both at the center of the main pulse, as well as on its trailing side and contributes practically nothing to the shift of the PA curve with respect to the intensity profile.*

Another issue related to aberration is mostly nomenclatural. In this paper I describe the origin of the delay-radius relation as the ‘straightening of electron trajectories’ when they are transformed from CF to IOF. Or, one can say the effect is due to the transformation of electron acceleration from the non-inertial CF to IOF. In the wording of HA the phase shift caused by these effects is described as ‘aberrational’ too (see eg. their Appendix F and G). An argument

that can (possibly) justify this is eq. (A1) (their eq. F1). The addition of velocities (aberration) given in this equation determines the electron velocity in IOF, which is next differentiated to obtain IOF acceleration. Of course, what really matters is not the fact that we add the corotation velocity, but the fact that the added velocity is time-dependent (or that CF is non-inertial). Since the phenomenon of aberration by itself refers only to the velocity of a reference-frame, and not to its acceleration, the term ‘aberration’ misses the essence of the effect, which is the *time-dependent nature* of the corotation velocity in (A1).

A word of comment on papers that have assumed that the PA curve is shifted *forward* in phase, just as the intensity profile does (eg. KD83; Xu et al. 1997; note that the work of KD83 was published in the pre-BCW era). If one corrects the analysis of KD83 for the direction of the PA shift, the altitude order of their four emission regions (see. their fig. 16) should be turned upside-down, ie. the region 4 should be at the top, region 3 below 4, etc.

Finally a note related to the high-energy emission. Electrons with Lorentz factors  $\gamma \simeq 10^6 - 10^7$  that move along the dipole axis trajectory with  $\rho_{rt} = R_{lc}/2$  and  $P \sim 0.1$  s emit curvature radiation that extends up to 0.1 – 100 MeV, respectively. This energy is too low for pair production (see fig. 7 in Dyks & Rudak 2002). However, this radiation may contribute to the observed X-rays and gamma-ray pulse profiles and spectra. In the numerical models of the high-energy emission from pulsars it is therefore necessary to calculate the curvature radiation using the radius of curvature of electron trajectory in the inertial observer frame.

## ACKNOWLEDGEMENTS

I thank B. Rudak for comments on the manuscript. This paper was supported by the grant N203 017 31/2872 of the Ministry of Science and Higher Education.

## REFERENCES

- Backer, D. C., Kulkarni, S. R., Heiles, C., Davis, M. M. & Goss, W. M., 1982, *Nature*, 300, 615  
 Barnard, J.J. 1986, *ApJ*, 303, 280  
 Blaskiewicz M., Cordes J.M., Wasserman I., 1991, *ApJ*, 370, 643 (BCW)  
 Braje, T.M., Romani, R.W., & Rauch, K.P. 2000, *ApJ*, 531, 447  
 Helfand, D. J., et al., 2006, *Nature*, 442, 892  
 Cheng, A. F., & Ruderman, M. 1979, *ApJ*, 229, 348  
 D’Angelo, C., & Rafikov, R.R. 2007, *Phys. Rev. D*, 75, 042002  
 Deutsch, A.J. 1955, *Ann. d’Astrophys.*, 18, 1  
 Dyks J., & Harding, A. K. 2004, *ApJ* 614, 869 (DH04)  
 Dyks, J., & Rudak, B. 2002, *A&A*, 393, 511  
 Dyks, J., Frackowiak, M., Słowiowska, A., et al., 2005, *ApJ* 633, 1101  
 Dyks J., Harding A.K., & Rudak, B. 2004a, *ApJ* 606, 1125  
 Dyks J., Rudak B., & Harding, A.K. 2004b, *ApJ* 607, 939 (DRH)  
 Dyks, J., Rudak, B., & Rankin, J.M. 2007, *A&A*, 465, 981 (DRR)  
 Everett J.E., & Weisberg J.M., 2001, *ApJ* 553, 341  
 Gil, J., & Krawczyk, A. 1997, *MNRAS*, 285, 561  
 Gonthier, P.L., & Harding, A.K. 1994, *ApJ*, 425, 767  
 Gupta, Y., & Gangadhara, R.T. 2003, *ApJ*, 584, 418  
 Hessels, J. W. T., Ransom, S. M., Stairs, I. H., Freire, P. C. C., Kaspi, V. M. & Camilo, F., 2006, *Science*, 311, 1901  
 Hibschan, J.A., & Arons, J. 2001, *ApJ*, 546, 382 (HA)  
 Johnston, S., Karastergiou, A., Mitra, D., & Gupta, Y. 2008, *MNRAS*, in press (astro-ph/0804.3838)  
 Karastergiou, A., & Johnston, S. 2007, *MNRAS*, 380, 1678  
 Kijak, J., & Gil, J. 1997, *MNRAS*, 288, 631  
 Komesaroff, M.M. 1970, *Nature*, 225, 612  
 Kramer, M., Lyne, A.G., O’Brien, J.T., et al. 2006, *Science*, 312, 549  
 Krishnamohan, S., & Downs, G.S. 1983, *ApJ*, 265, 372 (KD83)  
 Kunzl T., Lesch H., Jessner A., von Hoensbroech, 1998, *ApJ* 505, L139  
 Lai, D., Chernoff, D.F., & Cordes, J.M. 2001, *ApJ*, 549, 1111  
 Luo, Q., & Melrose, D. B. 1992, *MNRAS*, 258, 616  
 Lyubarsky, Y.E., 2002, *Proc. of the 270. WE-Heraeus Seminar*, eds. W. Becker, H. Lesch, & J. Trümper, MPE Report 278, 230  
 Melrose, D.B. 1979, *Austr. J. Phys.*, 32, 61  
 Mitra, D., & Seiradakis, J.H. 2004, *Proc. of the 6th Astronomical Conference*, ed. Laskarides, P., Editing Office of the Univ. of Athens, p. 205 (astro-ph/0401335)  
 Radhakrishnan, V., & Cooke, D.J. 1969, *Astrophys. Lett.*, 3, 225 (RC69)  
 Radhakrishnan, V., & Deshpande, A.A. 2001, *A&A*, 379, 551  
 Rankin, J.M. 1983, *ApJ*, 274, 333  
 Rankin, J.M., & Ramachandran, R. 2003, *ApJ*, 590, 411  
 Rankin, J.M., & Rathnasree, N. 1997, *J. Astrophys. Astron.*, 18, 91  
 Shitov, Yu.P. 1983, *Soviet. Astron.*, 27, 314  
 Spitkovsky, A. 2008, *AIP Conference Proceedings*, 983, 20  
 Takata, J., Shibata, S., Hirotani, K., & Chang, H.-K. 2006, *MNRAS*, 366, 1310  
 Thomas, R.M.C., & Gangadhara, R.T. 2005, *A&A*, 437, 537  
 von Hoensbroech, A., & Xilouris, K.M. 1997, *A&A*, 324, 981  
 Xilouris, K. M., Kramer, M., Jessner, A., et al. 1998, *ApJ*, 501, 286  
 Xu, R.X., Qiao, G.J., & Han, J.L. 1997, *A&A*, 323, 395

## APPENDIX A: SIMPLE DERIVATION OF EQ. (1)

Let us consider the geometry shown in Fig. A1. The three positions A', P', and B' of a point at the light cylinder are separated by the same path increment  $s \simeq R_{lc}\delta$  so that the triangles OA'P' and OP'B' are identical. As soon as we mark in this figure some arbitrary position, say A, of an electron that is moving radially in the corotating frame, the trajectory APB of the electron becomes uniquely determined. This is because: 1) the electron also moves with the speed of light  $c$  (as the point at the light cylinder does), so that we must have  $|AP| = |PB| = s$  and 2) the electron has the same

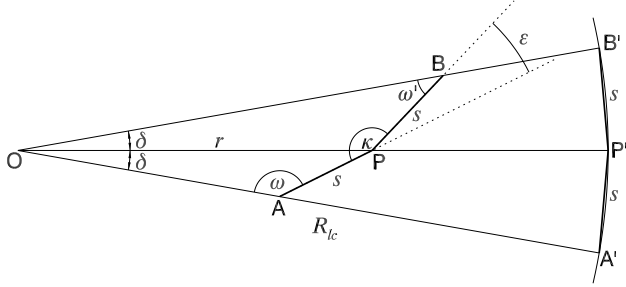


**Figure A1.** Trajectory APB of a relativistic electron that is moving along the straight dipole axis in the corotating frame. Rotation axis is perpendicular to the page at O. The points A', P', and B' present locations of a point corotating at the light cylinder. The diagram is used in the school-style derivation of eq. (1) (Appendix A).

angular velocity  $\Omega$  so that both AP and PB must subtend their respective angles  $\delta$ .

The electron trajectory has a radius of curvature  $\rho_{rt} = s/\varepsilon$  (for elementary reasons), where  $\varepsilon = \pi - \kappa$  and  $\kappa$  is the angle between AP and PB. For the quadrangle OAPB we can write  $2\delta + \omega + \kappa + \omega' = 2\pi$  which implies  $\varepsilon = 2\delta + \omega + \omega' - \pi$ . The sine theorem for the OPB triangle gives  $\sin \omega' = r \sin(\delta)/s \simeq r\delta/s \simeq r/R_{1c}$ , i.e.  $\omega' \simeq \arcsin(r/R_{1c}) \simeq r/R_{1c}$ . For the OAP triangle one has  $\sin \omega = r \sin(\delta)/s \simeq r/R_{1c}$  (same as for  $\omega'$ ) but this time  $\omega$  is in the range  $\pi/2 < \omega < \pi$  (see Fig. A1) so that  $\omega = \pi - \arcsin(r/R_{1c}) \simeq \pi - r/R_{1c}$ . Thus we have  $\varepsilon \simeq 2\delta \simeq 2s/R_{1c}$  so that  $\rho_{rt} = s/\varepsilon \simeq R_{1c}/2$ .

A formal derivation of eq. (1) assumes that the electron velocity is given by:

$$\vec{v} \simeq c\hat{b} + \vec{\Omega} \times \vec{r}, \quad (\text{A1})$$

where  $\hat{b}$  is a unit vector along the local direction of  $\vec{B}$ , and the tiny difference between the electron speed along  $\hat{b}$  and  $c$  is neglected (hence the ‘ $\simeq$ ’ sign). The electron acceleration is then:

$$\vec{a} = \frac{d\vec{v}}{dt} = c\frac{d\hat{b}}{dt} + \vec{\Omega} \times \frac{d\vec{r}}{dt} = c\frac{d\hat{b}}{dt} + \vec{\Omega} \times \vec{v} = \quad (\text{A2})$$

$$= c\frac{\partial \hat{b}}{\partial t} + c(\vec{v} \cdot \nabla)\hat{b} + c\vec{\Omega} \times \hat{b} + \vec{\Omega} \times (\vec{\Omega} \times \vec{r}), \quad (\text{A3})$$

where the Lagrange derivative of  $\hat{b}$  in (A2) has been expressed explicitly in (A3) and  $\vec{v}$  from (A1) has been inserted into the last term of (A2).

The factor  $\partial \hat{b}/\partial t$  represents the rotation of essentially radial unit vector  $\hat{b}$  with angular velocity  $\Omega$  and therefore the first term has the magnitude of  $\Omega c$ . The second term in eq. (A3) represents the contribution to acceleration that results from curvature of magnetic field lines and is zero at the dipole axis (solely this term fully represents the original model of the RC69). The third term has the same magnitude as the first one:  $|c\vec{\Omega} \times \hat{b}| \simeq \Omega c$ . The last term has the magnitude of  $\Omega$  times the local corotation velocity  $\vec{v}_{\text{crt}} = \vec{\Omega} \times \vec{r}$  and it is negligible at low altitudes where  $v_{\text{crt}} \ll c$ . Thus,  $|\vec{a}| \simeq 2\Omega c$  and  $\rho_{rt} \simeq c^2/a \simeq R_{1c}/2$ .

For  $\alpha \neq 0$  (and  $\zeta = \alpha$ ) the two non-zero terms in eq. A3 (and therefore  $\vec{a}$ ) are smaller by a factor of  $\sin \alpha$ , so that  $\rho_{rt}$  is larger by  $1/\sin \alpha$ . The zero-curvature regions are located closer to the dipole axis by the  $\sin \alpha$  factor. However, the

delay-radius relation retains its usual form ( $\alpha$ -independent), because the  $\sin \alpha$  factor is cancelled by the ‘not a great circle’ effect.

Yet another derivation of eq. (1) can be found in Thomas & Gangadgara (2005) (see their eq. 29).

## APPENDIX B: ABERRATION AND PROPAGATION TIME DELAYS

The aberration is understood as the change of emission direction of radio waves caused by the transition from the Lorentz frame instantaneously comoving with a corotating emission point to the inertial observer frame (IOF). I assume that in the corotating frame (CF) the radio waves are emitted in the direction  $\vec{k}'$  which is tangential to the direction of dipolar magnetic field ( $\vec{k}' = \pm \vec{B}/|\vec{B}|$ ). Then, in the IOF the emission occurs in the direction:

$$\vec{k} = \frac{\vec{k}' + [\gamma_{\text{crt}} + (\gamma_{\text{crt}} - 1)(\vec{\beta}_{\text{crt}} \cdot \vec{k}')/\beta_{\text{crt}}^2]\vec{\beta}_{\text{crt}}}{\gamma_{\text{crt}}(1 + \vec{\beta}_{\text{crt}} \cdot \vec{k}')} \quad (\text{B1})$$

where  $\gamma_{\text{crt}} = (1 - \beta_{\text{crt}}^2)^{-1/2}$ , and  $\vec{\beta}_{\text{crt}} \equiv \vec{v}_{\text{crt}}/c = \vec{\Omega} \times \vec{r}/c$ . Eq. (B1) is just the general Lorentz transformation for an arbitrary velocity vector  $\vec{v}$ , in which I substituted  $\vec{k} = \vec{v}/c$  and  $\vec{k}' = \vec{v}'/c$ .

For low emission altitudes ( $r \ll R_{1c}$ ) and near the dipole axis (small angle approximation) eq. (B1) can be considerably simplified because  $\vec{k}'$  is not far from radial and  $\vec{v}_{\text{crt}}$  is small and purely azimuthal. Using the spherical coordinates  $(r, \phi, \theta)$ , with  $\hat{z}$ -axis along  $\vec{\Omega}$  and with the azimuth  $\phi$  increasing in the direction of the corotation velocity  $\vec{v}_{\text{crt}} = \vec{\Omega} \times \vec{r}$  the aberration formula becomes:

$$\begin{aligned} \vec{k} = (1, \phi_k, \theta_k) &\approx (1, \phi'_k + r/R_{1c}, \theta'_k) = \\ &= \vec{k}' + (0, r/R_{1c}, 0), \end{aligned} \quad (\text{B2})$$

which means that in our specific case the aberration basically rotates the emission direction forward in phase by  $r/R_{1c}$  rad, regardless of the emission colatitude (DRH). Note that eq. (B2) refers to the unit vectors of emission direction after they have been parallel-shifted to the origin of the coordinates’ frame:  $\vec{k} = (1, \phi_k, \theta_k)$ ,  $\vec{k}' = (1, \phi'_k, \theta'_k)$ .

Propagation time delays (also called ‘retardation’) refer to the travel time of radio waves within the pulsar magnetosphere: radiation emitted deeper in the magnetosphere will be detected later than the simultaneous emission from high altitudes. The delays are taken into account through the reference to the center of the neutron star (NS). Let us consider a point located at the radial position  $\vec{r}$  at the instant  $t_{\text{em}}$  when it is emitting towards an observer. Under normal conditions such a point is located closer to the observer than the NS center. Radiation emitted from this point will therefore be detected *earlier* by  $\vec{r}(t_{\text{em}}) \cdot \hat{n}_{\text{obs}}/c$  than an imaginary signal simultaneously emitted from the center of the NS. Here  $\vec{r}(t_{\text{em}}) \cdot \hat{n}_{\text{obs}}$  is a projection of  $\vec{r}$  (taken at the instant of emission) on the observer’s line of sight (defined by the unit vector  $\hat{n}_{\text{obs}}$ ) and I assume that the radio waves travel at the speed of light  $c$  (dispersion is ignored). Note that the propagation time advance/delay is *not* independent of aberration: to find  $\vec{r}(t_{\text{em}})$  at the moment of emission, we first need to know the aberrated emission direction  $\vec{k}(\vec{r})$ . However, since the angle between  $\vec{r}(t_{\text{em}})$  and  $\hat{n}_{\text{obs}}$  is small, in the lowest

order approximation the propagation time advance simply becomes:  $\vec{r}(t_{\text{em}}) \cdot \hat{n}_{\text{obs}}/c \approx r/c$  and the associated phase advance is  $r/R_{\text{lc}}$ , just as in the case of aberration.

This paper has been typeset from a  $\text{\TeX}/\text{\LaTeX}$  file prepared by the author.